

## THE VISIBLE DIFFUSE REFLECTANCE SPECTRUM IN RELATION TO THE COLOR AND CRYSTAL PROPERTIES OF HEMATITE

JOSE TORRENT\* AND VIDAL BARRON

Departamento de Ciencias y Recursos Agrícolas y Forestales, Universidad de Córdoba, Apdo. 3048, 14080 Córdoba, Spain

**Abstract**—Hematite ( $\alpha\text{-Fe}_2\text{O}_3$ ) possesses distinct spectral properties which facilitate its identification in mineral mixtures. This paper reports the relationships between the visible diffuse reflectance (DR) spectrum and the color and crystal properties of a group of 81 natural and synthetic hematites. The visible DR spectra for powdered hematite samples diluted to 4 wt.% with  $\text{BaSO}_4$  white standard were recorded and used to calculate the corresponding Munsell colors. The second derivative of the Kubelka-Munk function of the DR was used to estimate the position and intensity of the main absorption bands, which occurred at  $\sim 435$ ,  $\sim 485$  and  $\sim 545$  nm. The Munsell hue ranged from 9.5P to 5.3YR and was negatively correlated with the position of the  $\sim 545$  nm band, so it became yellower as the band shifted to shorter wavelengths (higher energies). The Munsell value, which ranged from 4.9 to 8.6, and chroma, which ranged from 14 to 8.3, were negatively and positively correlated, respectively, with the intensity of the  $\sim 545$  nm band, the position of which exhibited a weak negative correlation with the degree of Al substitution ( $x$ ). The position and intensity of this band also exhibited a weak negative correlation with the specific surface area (SSA); both, however, were uncorrelated with domain shape as measured by the ratio between the X-ray mean coherence lengths (MCLs) in the [110] and [104] directions. The properties of the  $\sim 435$  and  $\sim 485$  nm bands were unrelated to  $x$ , SSA or  $\text{MCL}_{104}/\text{MCL}_{110}$ . The negative relationship between the position of the  $\sim 545$  nm band and  $x$  does not support the assignment of this band to the  $2(6A_1) \rightarrow 2(^4T_{1g}(^4G))$  electron pair transition (EPT), which relates to the  $\text{Fe}^{3+}\text{—Fe}^{3+}$  magnetic coupling between face-sharing octahedra. The  $\sim 485$  nm band might reflect a 'goethitic' structural component in Fe-defective hematites as it appears at the same wavelength as the hypothetical EPT related to  $\text{Fe}^{3+}\text{—Fe}^{3+}$  magnetic coupling between edge-sharing octahedra in goethite ( $\alpha\text{-FeOOH}$ ).

**Key Words**—Al Substitution, Color, Diffuse Reflectance, Hematite.

### INTRODUCTION

Hematite exhibits characteristic spectral properties that facilitate its identification in soils (e.g. Torrent *et al.*, 1983), sediments (e.g. Torrent and Schwertmann, 1987) and planetary surfaces (e.g. Morris *et al.*, 1993), as well as its discrimination from other Fe oxides and hydroxides (Malengreau *et al.*, 1996; Scheinost *et al.*, 1998; Scheinost and Schwertmann, 1999). Various regions of its spectrum have been analyzed for these purposes. For instance, the presence of red (pigmentary) hematite in the bright regions of Mars was inferred from some inflections in the visible spectrum (e.g. Morris *et al.*, 1997); also, coarse-grained ( $>5\text{--}10$   $\mu\text{m}$ ) hematite was identified in the Mars Sinus Meridiani on the basis of vibrational absorption features centered in the IR (300, 450 and  $>525$   $\text{cm}^{-1}$ ) (Christensen *et al.*, 2000).

Particle size and shape, and crystallochemical properties, exert a strong influence on the hematite spectrum. For instance, Morris *et al.* (1992) found Al substitution to affect the position of the ligand-field  $6A_1 \rightarrow ^4T_{1g}$  transition (centered in the near IR) in  $<0.5$   $\mu\text{m}$  hematite crystals. Therefore, spectral properties might, in princi-

pie, be useful to investigate some hematite properties.

The color of hematite results from several ligand-field transitions within the visible range ( $\sim 380\text{--}770$  nm) and the strong influence of ligand-to-metal charge-transfer transitions at  $\sim 250$  nm in the UV (Sherman and Waite, 1985). Diffuse reflectance spectra for hematite show that the position and intensity of the bands corresponding to ligand field transitions vary widely (Scheinost *et al.*, 1998), and so does color (Scheinost and Schwertmann, 1999). Several studies suggest that these variations are caused by particle size (e.g. Morris *et al.*, 1985), Al substitution (Barron and Torrent, 1984), the presence of structural P (Galvez *et al.*, 1999) and, possibly, X-ray domain shape (Morris *et al.*, 1992). Unfortunately, some of these factors are covariant (e.g. Al substitution and particle shape) and most relevant studies have focused on a few series of samples synthesized in a similar way (e.g. Van San *et al.*, 2001). The available information is thus of limited help in the identification and characterization of hematite in single- and multi-mineral samples. In this work, the visible DR spectra for a large number of widely different synthetic and natural hematites were used to examine (1) the relationships between color and spectral properties, and (2) the effect of crystal properties on the hematite spectrum.

\* E-mail address of corresponding author:

torrent@uco.es

DOI: 10.1346/CCMN.2003.0510307

## MATERIAL AND METHODS

## Samples

The following 55 synthetic hematites were used: (1) series A, B, C, D, E and S (data in Barrón *et al.*, 1988); (2) series B, CT, H, MC, OX, SE and TR (data in Colombo *et al.*, 1994), and (3) samples S1, S2, S3, S4, S6, S7 and S8 (data in Torrent and Schwertmann, 1987). These series had been prepared under substantially different conditions (pH, concentration of organic ligands, initial Al/Fe ratio, etc.). The 26 natural hematite-containing samples used included (1) samples 5 and 10 from the Atlantis II Deep, Red Sea (Schwertmann *et al.*, 1998); (2) two ground quartz crystals with hematite inclusions (samples Jac 1, Jac 2); (3) three hematite-colored, ground altered basalts from the Giants Causeway area, Northern Ireland (Ir1, Ir2, Ir3); (4) 14 ground samples from red beds of different ages (from Permian to Miocene) and two saprolites (data in Torrent and Schwertmann, 1987), and (5) two hydrothermal specular hematites (Spec2, Spec3), and a fibrous nodular hematite (Spec4) from three unknown locations in Spain. Table 1 summarizes the properties of the samples.

## Diffuse reflectance measurements

Diffuse reflectance spectra were recorded from 380 to 900 nm in 0.5 nm steps at a scan speed of 30 nm min<sup>-1</sup> using a Varian Cary 1E spectrophotometer equipped with a BaSO<sub>4</sub>-coated integrating sphere 73 mm in diameter. Powdered (<10 μm) samples were pressed by hand into the 8 × 17 mm rectangular holes of white

plastic holders (thickness: 2.5 mm) at a pressure >5 bar. The resulting mounts were self-supporting, thus allowing holders to be placed vertically without the powder falling into the sphere. For measurement, pure hematite or hematite-containing samples were thoroughly (but gently) ground with white standard BaSO<sub>4</sub> (Merck DIN 5033) to make the proportion of hematite 4% of the total sample weight (300 mg). Natural samples containing <4 wt.% hematite were not diluted. In order to estimate the scattering coefficient, *S*, defined in the Kubelka-Munk formalism for BaSO<sub>4</sub>, the reflectance spectra of several thin layers of BaSO<sub>4</sub> over a black background (black paper with reflectance <6% in the visible range) were acquired. The value of *S* was then taken as the slope of the regression line of *Sd* (*d* being the thickness of the BaSO<sub>4</sub> layer) against *d*, with *Sd* given by the equation (Kortüm, 1969)

$$Sd = \left[ \frac{1}{R_\infty} - R_\infty \right]^{-1} \left[ \ln \frac{(R - \frac{1}{R_\infty})(R_g - R_\infty)}{(R_g - \frac{1}{R_\infty})(R - R_\infty)} \right] \quad (1)$$

where, for each wavelength, *R*, *R*<sub>∞</sub> and *R*<sub>g</sub> are the absolute reflectances of (1) a thin BaSO<sub>4</sub> layer over the black background, (2) a thick layer of BaSO<sub>4</sub>, and (3) the black background, respectively. The value of *d*, which ranged from 0.14 to 0.37 mm, was estimated with the aid of a microscope.

## Spectral parametrization and calculations

The Kubelka-Munk (K-M) remission function (Kubelka and Munk, 1931) at each wavelength, λ, was calculated from

Table 1. Selected properties of hematites.

	Minimum	Maximum	Mean	Standard deviation
Al substitution (mole fraction)	0.00	0.143	0.049	0.044
SSA (m <sup>2</sup> g <sup>-1</sup> )	2	116	34	31
MCL <sub>110</sub> /MCL <sub>104</sub>	0.74	5.26	1.42	0.62
Band at ~435 nm				
Position (nm) <sup>1</sup>	421	453	433	6
Intensity (× 10 <sup>-4</sup> ) <sup>1</sup>	0.1	7.7	2.7	2.2
Band at ~485 nm				
Position (nm) <sup>1</sup>	475	503	488	6
Intensity (× 10 <sup>-4</sup> ) <sup>1</sup>	0.1	4.1	1.2	0.9
Band at ~545 nm				
Position (nm) <sup>1</sup>	530	572	544	9
Intensity (× 10 <sup>-4</sup> ) <sup>1</sup>	0.4	19.5	8.8	5.5
Munsell notation <sup>2</sup>				
Hue	9.5P	5.3YR	0.1YR <sup>3</sup>	4.7 <sup>3</sup>
Value	4.9	8.6	6.9	0.8
Chroma	1.4	8.3	5.2	2.0

<sup>1</sup> From the second-derivative of the Kubelka-Munk function for samples containing 4 wt.% hematite

<sup>2</sup> For samples containing 4 wt.% hematite; includes a few natural samples with <4 wt.% hematite

<sup>3</sup> For descriptive statistics a numerical scale is used, on which -10 is assigned to 10P, 0 to 10RP, 10 to 10R, and 20 to 10YR

$$F(R_\infty) = \frac{K}{S} = \frac{(1 - R_\infty)^2}{2R_\infty} \quad (2)$$

where  $K$  and  $S$  are the absorption and scattering coefficients defined by the theory, respectively, and  $R_\infty$  is the reflectance of a thick layer of sample ( $>2$  mm for samples containing Fe oxides). The first and second derivatives of the K-M function were calculated by using a cubic spline procedure (Press *et al.*, 1992) adapted to BASIC programming language by the authors. This method involves end-to-end joining of a number of cubic polynomial segments based on a certain number of adjacent data points with continuity in the first and second derivative at the joints. Segments with 24 data points were adopted because they provided second-derivative spectra with both well-resolved absorption bands and relatively low background noise. The minima in the second-derivative spectrum were assumed to coincide with the positions of the different absorption bands. The difference in ordinate between the minimum and the next maximum at a longer  $\lambda$ , which is referred to hereafter as 'band intensity', was used as a proxy for the true band amplitude (see *e.g.* Figure 6 in Scheinost *et al.*, 1998).

The CIE 1931 color-matching functions,  $\bar{x}(\lambda), \bar{y}(\lambda), \bar{z}(\lambda)$ , weighted by the relative spectral radiant power distribution,  $C(\lambda)$ , of CIE Standard Illuminant,  $[C(\lambda)\bar{x}(\lambda), C(\lambda)\bar{y}(\lambda), C(\lambda)\bar{z}(\lambda)]$  (Figure 1), were used to calculate the tristimulus values,  $X, Y, Z$ , using the equations  $X = \int R(\lambda)C(\lambda)\bar{x}(\lambda)d\lambda$ ,  $Y = \int R(\lambda)C(\lambda)\bar{y}(\lambda)d\lambda$ , and  $Z = \int R(\lambda)C(\lambda)\bar{z}(\lambda)d\lambda$ , where  $R(\lambda)$  is the reflectance at  $\lambda$ . The data tabulated by Wyszecki and Stiles (1982) at 5 nm intervals in the 380–770 nm range were used in all these calculations. The chromaticity coordinates,  $x = X/(X+Y+Z)$ ,  $y = Y/(X+Y+Z)$ ,  $z = Z/(X+Y+Z)$ , were

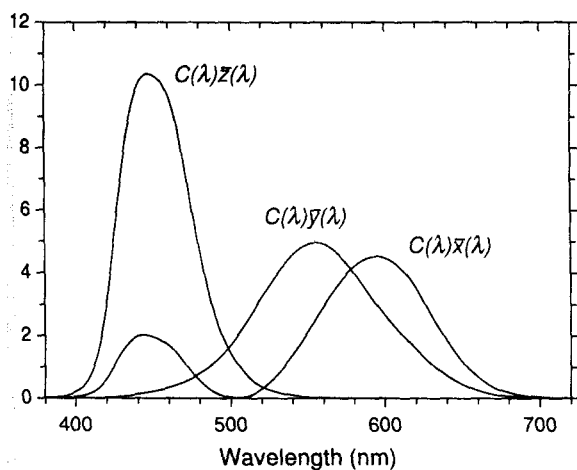


Figure 1. CIE 1931 color-matching functions as weighted by the relative spectral radiant distribution of Illuminant C. Numbers on the y axis correspond to the weighting factor used when reflectance (%) values are taken at 5 nm intervals.

converted into the hue, value and chroma of the Munsell notation with the aid of free software downloaded from Munsell Color's website ([www.Munsell.com](http://www.Munsell.com)).

## RESULTS AND DISCUSSION

### *Relationships between color and the second-derivative spectrum*

The mean Munsell hue was 0.1YR (range 9.5P–5.3YR), the mean Munsell value 6.9 (range 4.9–8.6), and the mean Munsell chroma 5.2 (range 1.4–8.3) (Table 1). Relative to the group of hematites studied by Scheinost and Schwertmann (1999), this group extends more into the purple region and is shifted to higher values by an average of about three units; on the other hand chroma ranges are similar. The discrepancy in value was to be expected because measurements were made on samples containing 4 wt.% or less hematite. In this respect, it can easily be shown, both experimentally and by using calculations based on the K-M theory, that diluting pure hematite with a white standard or a colorless mineral matrix (*e.g.* quartz, kaolinite) results in a slight yellow shift, little change in chroma, and a marked increase in the lightness (value) for the sample (Barrón and Torrent, 1986). In summary, dilution was expected to increase the Munsell value by about three units and to have no substantial effect on hue or chroma, and hence on relative differences among samples. The relatively minor disadvantages of dilution were offset by the absence of problems due to particle orientation (leading to specular reflection) and saturation of the K-M function typical of pure samples (Kortüm, 1969; Hapke, 1993).

Color was influenced by three main absorption bands, which, based on the second-derivative spectra, occurred at ~435, ~485 and ~545 nm (Table 1, Figure 2). The band at ~545 nm, which was assigned to the  $2(6A_1) \rightarrow 2(4T_{1g}(4G))$  EPT by Sherman and Waite (1985), was the strongest, followed by the ~435 nm band, which corresponds to the  $6A_1 \rightarrow 4E; 4A_1$  transition (Sherman and Waite, 1985), and the band at ~485 nm, the origin of which is discussed below.

Table 2 shows the linear correlation coefficients between selected spectral and color variables (for the Munsell hue a numerical scale was used in which 10P = -10, 5RP = -5, 10RP = 0, 5R = 5, 10R = 10, and 5YR = 15). The hue was correlated negatively with the position of the ~545 nm band, which accounted for 81% of the variance of hue when a quadratic relationship was fitted to the data (Figure 3). This relationship is due to the different position of the maxima in the  $C(\lambda)\bar{y}(\lambda)$  and the  $C(\lambda)\bar{x}(\lambda)$  functions (~555 and ~600 nm, respectively; Figure 1). Thus, as the absorption band shifts from ~530 nm to higher  $\lambda$  values,  $Y$  (or  $y$ ) decreases to a greater extent than  $X$  (or  $x$ ) and the hue becomes more purple. This is apparent from the region between 5YR

and 5RP in the  $(x,y)$  chromaticity diagram (Figure 4), where small decreases in  $y$  result in marked shifts to more purple hues (and small increases in  $y$  result in marked shifts to yellower hues), whereas changes in  $x$  have little effect on hue. The hue was not correlated with the intensity of the  $\sim 545$  band. The reason for this is unclear but it may be that the relative values of  $y$  and  $x$  are less sensitive to band intensity than band position in a region where the maximum values of the  $C(\lambda)\bar{y}(\lambda)$  and the  $C(\lambda)\bar{x}(\lambda)$  functions are close.

Positive, significant correlations between the hue and the intensity of the  $\sim 435$  and  $\sim 485$  nm bands were observed because  $Z$  tends to decrease more than either  $X$  or  $Y$  as the intensity of these bands increases. This

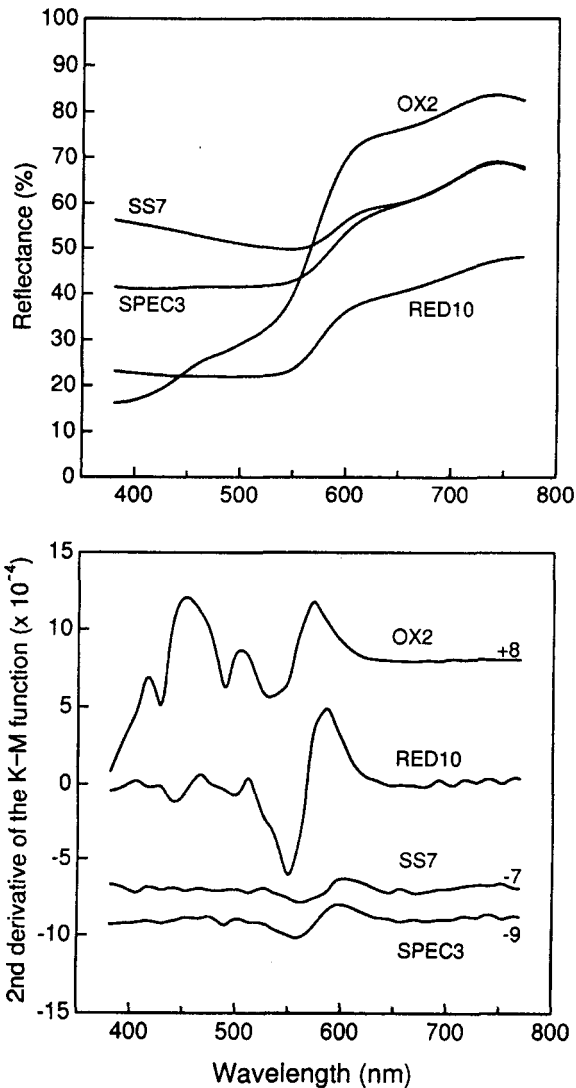


Figure 2. Reflectance spectrum (top) and second-derivative of the Kubelka-Munk (K-M) function of the spectrum (bottom) for selected hematite samples. OX2: synthetic, Al mole fraction ( $x$ ) = 0.05, SSA =  $84 \text{ m}^2 \text{ g}^{-1}$ ; SS7: synthetic,  $x = 0$ , SSA =  $3 \text{ m}^2 \text{ g}^{-1}$ ; RED10: red bed of Keuper age,  $x = 0.05$ , calculated SSA =  $14 \text{ m}^2 \text{ g}^{-1}$ ; SPEC3, ground specularite of hydrothermal origin,  $x = 0$ .

Table 2. Single correlation coefficients for absorption band properties and Munsell hue, value and chroma.

	Hue	Value	Chroma
Band at $\sim 435$			
Position	-0.23*	-0.33 <sup>†</sup>	0.24*
Intensity	0.51 <sup>#</sup>	-0.35 <sup>†</sup>	0.58 <sup>#</sup>
Band at $\sim 485$			
Position	0.35 <sup>#</sup>	-0.17 ns	0.22 ns
Intensity	0.37 <sup>#</sup>	-0.29 <sup>†</sup>	0.60 <sup>#</sup>
Band at $\sim 545$			
Position	-0.82 <sup>#</sup>	0.02 ns	-0.54 <sup>#</sup>
Intensity	0.11 ns	-0.78 <sup>#</sup>	0.74 <sup>#</sup>

\*, <sup>†</sup>, <sup>#</sup> Significant at the 0.05, 0.01 and 0.001 probability levels, respectively

results in increases in  $x$  and  $y$ , and hence in shifts to less purple (yellower) hues. The position of these bands has little influence on hue because  $Z$  is always more markedly affected than either  $X$  or  $Y$  over the range where these bands appear.

Value was negatively correlated ( $r = -0.78$ ;  $P < 0.001$ ) with the intensity of the  $\sim 545$  nm band because this band has a strong effect on  $Y$ , which is directly related to value (Value  $\approx 2.5Y^{1/3} - 1.7$ ; Wyszecki and Stiles, 1982).

Chroma was positively correlated with the intensity of the  $\sim 435$ ,  $\sim 485$  and, especially, the  $\sim 545$  nm band (Figure 5). This was to be expected because an increase in intensity of any of these bands results in a reduction of  $Y$  and  $Z$  relative to  $X$ , *i.e.* an increase in  $x$ , which in turn causes an increase in chroma in the portion of interest of the  $(x,y)$  chromaticity diagram.

In summary, the color of hematite is strongly influenced by the position of the  $\sim 545$  nm band, and, to a

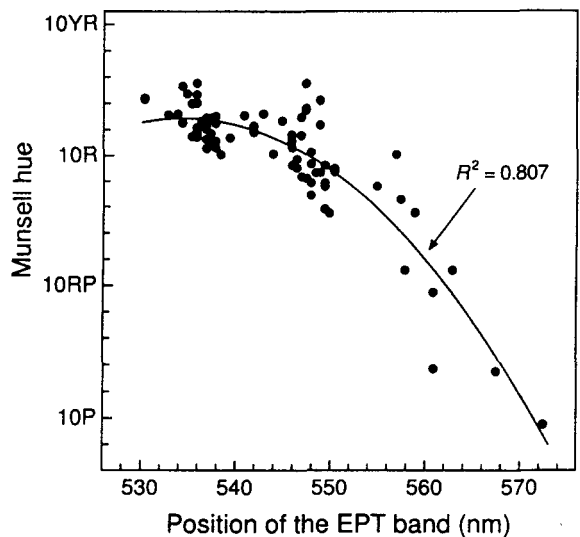


Figure 3. Munsell hue in relation to the position of the band assigned to the electron pair transition (EPT).

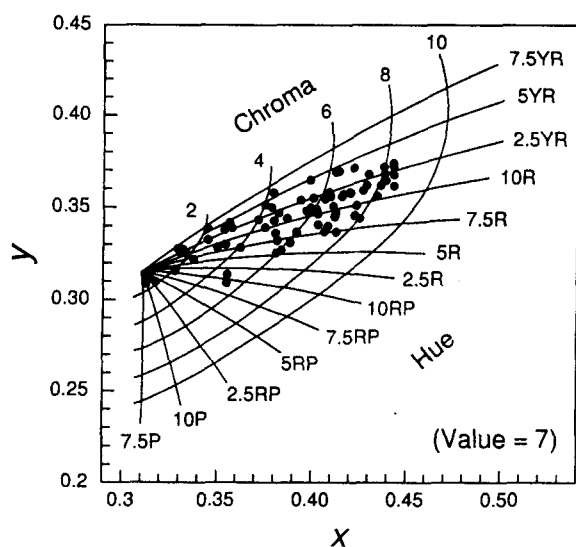


Figure 4. CIE 1931 ( $x,y$ ) chromaticity diagram at value 7 of the Munsell system.

lesser extent, the position and intensity of the  $\sim 435$  and the  $\sim 485$  bands.

*Relationships between crystallochemical and morphological properties and the second-derivative spectrum*

Table 3 shows the Pearson correlation coefficients for the linear regressions among absorption band properties, the degree of Al substitution, specific surface area (SSA), and the ratio between the mean coherence lengths normal to the (110) and (104) planes ( $MCL_{110}/MCL_{104}$ ). Such a ratio increases as particles become more platy, which generally corresponds to an increase in the area of the (001) and (104) planes relative to other crystal faces. The regression analysis suggests that Al substitution

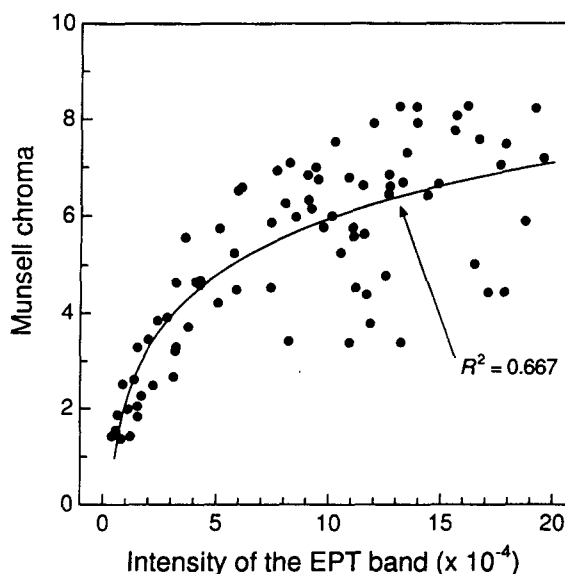


Figure 5. Munsell chroma in relation to the intensity of the band assigned to the EPT at  $\sim 545$  nm.

influences the position of the  $\sim 545$  nm band and hence hue, but does not seem to influence value or chroma. This band exhibits a slight tendency to shift to a shorter wavelength (higher energy) as Al substitution increases (Figure 6). The ligand field theory predicts an increase in the transition energy of the  $2(6A_1) \rightarrow 2(4T_{1g}(4G))$  EPT when the  $10Dq$  parameter decreases. Because  $10Dq$  is inversely proportional to the fifth power of the Fe–O distance (Burns, 1993), one would expect the reduction in unit-cell edge length caused by Al substitution to result in a lower energy for this transition, a contention not supported by Figure 6. The positive correlation between EPT energy and Al substitution was also observed in series of hematites prepared by thermal treatment of lepidocrocite (van San *et al.*, 2001), in

Table 3. Single correlation coefficients for absorption band, color and crystal properties.

	Al substitution (mole fraction)	SSA ( $m^2 g^{-1}$ )	$MCL_{110}/MCL_{104}$
Band at $\sim 435$ nm			
Position	0.02 ns	-0.26 ns	-0.17 ns
Intensity	-0.01 ns	0.00 ns	0.01 ns
Band at $\sim 485$ nm			
Position	-0.03 ns	0.06 ns	-0.06 ns
Intensity	-0.01 ns	0.00 ns	-0.15 ns
Band at $\sim 545$ nm			
Position	-0.36 <sup>†</sup>	-0.46 <sup>#</sup>	-0.09 ns
Intensity	0.04 ns	-0.40 <sup>†</sup>	-0.15 ns
Al substitution		0.37 <sup>†</sup>	0.18 ns
SSA			0.04 ns
Hue	0.30*	0.35 <sup>†</sup>	0.22 ns
Value	-0.00 ns	0.42 <sup>#</sup>	-0.05 ns
Chroma	0.14 ns	-0.04 ns	-0.30*

\*, <sup>†</sup>, <sup>#</sup> Significant at the 0.05, 0.01 and 0.001 probability levels, respectively

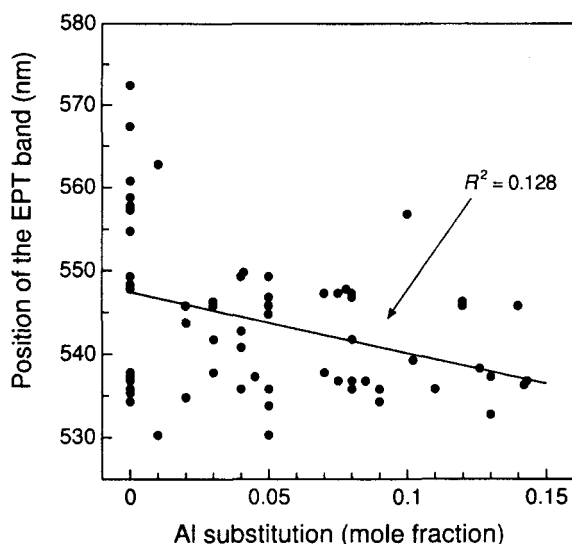


Figure 6. Position of the band assigned to the EPT in relation to the degree of Al substitution.

hematites obtained by homogeneous precipitation of oxinates (da Costa *et al.*, 2002), and in goethite series prepared in various ways (Scheinost *et al.*, 1999). By contrast, as predicted by the ligand field theory, the energy of the  $6A_1 \rightarrow 4T_{1g}$  single-ion transition ( $\lambda = 850\text{--}920\text{ nm}$ ) increases with Al substitution in both hematite (Morris *et al.*, 1992) and goethite (Scheinost *et al.*, 1999).

The position of the  $\sim 545\text{ nm}$  band shifts to a shorter wavelength (higher energy) with increasing SSA (*i.e.* decreasing particle size) (Table 3, Figure 7). This correlation is weak and does not necessarily reflect a cause-effect relationship because Al substitution and SSA are covariant ( $r = 0.37$ ;  $P < 0.01$ ). Separating the

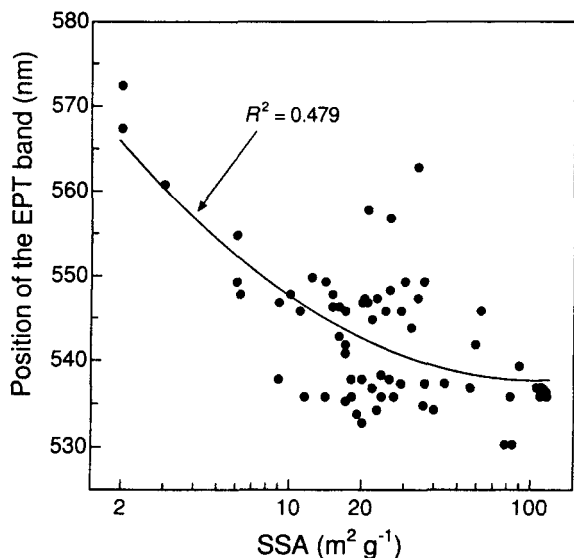


Figure 7. Position of the band assigned to the EPT in relation to specific surface area (SSA).

individual effects of Al substitution and SSA on the position of this band is difficult because Al influences hematite particle size and shape, making particles thinner in the [001] direction (Cornell and Schwertmann, 1996). Therefore, the way particle size affects the energy of the EPT is difficult to explain.

The relationship between SSA and the  $\sim 545\text{ nm}$  band position results in a slight, but significant relationship between SSA and hue ( $r = 0.35$ ;  $P < 0.01$ ), hue becoming yellower with increasing SSA, *i.e.* with decreasing particle size, and becoming more purple with decreasing SSA, *i.e.* with increasing particle size (Figure 8). This is consistent with the observation that  $\mu\text{m}$ -sized hematite particles (*e.g.* those prepared by hydrolysis of Fe(III) salts in highly alkaline solutions) exhibit dark purple colors. The influence of particle size on hematite color was discussed to some extent by Morris *et al.* (1985). Basically, in the violet and blue regions, where absorption is strong, reflectivity increases with increasing particle size because the regular reflection increases according to the Fresnel equation. In addition, regular reflection is expected to increase substantially with increasing size because large hematite crystals tend to have smooth faces. At longer wavelengths, where absorption is weak, reflectivity decreases with increasing size when the dimensions are greater than the wavelength, but increases with increasing size for very small particles (Kortüm, 1969; Hapke, 1993). However, aggregation, particularly in small particles, can strongly alter these relations (Hapke, 1993). In practice, by mathematically manipulating the reflectance spectrum according to these principles, the calculated hematite color should become more purple as particle size increases. This can be demonstrated easily by applying the following transformation to reflectance values:

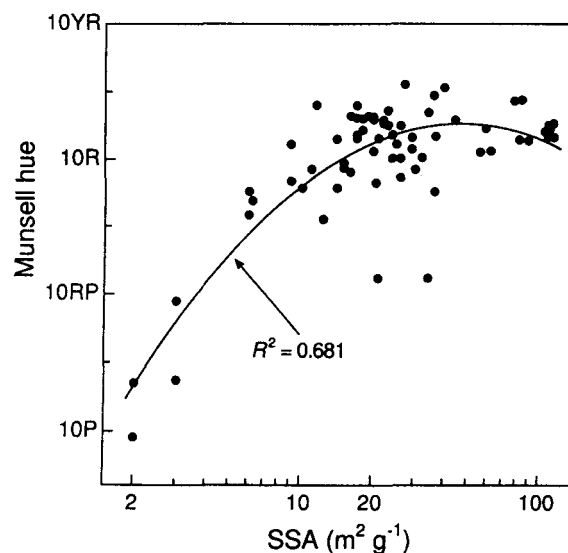


Figure 8. Munsell hue in relation to specific surface area (SSA).

$$R_2(\lambda) = R_1(\lambda)[1 + aF(R_\infty)S(\lambda)] \quad (3)$$

where  $R_2(\lambda)$  is the transformed reflectance,  $R_1(\lambda)$  the original reflectance,  $a$  is a parameter,  $F(R_\infty)$  the K-M function, and  $S(\lambda)$  the scattering coefficient. The  $F(R_\infty)S(\lambda)$  product is equal to  $K$ , the absorption coefficient of the K-M theory (equation 2). Therefore, equation 3 simply states that the increase in regular reflection brought about by an increase in size results in an increase in reflectance that is proportional by a factor  $a$  to the absorption coefficient of the sample. It must be noted that equation 3 is based on two assumptions, namely: (1) that  $K$  is proportional to the true absorption coefficient of the sample in transmission, which is not entirely true (Hapke, 1993), and (2) that  $S$  does not differ substantially from  $S$  for the diluent, which can be calculated with some accuracy by regression analysis based on equation 1 [for the  $\text{BaSO}_4$  standard used in our measurements,  $S(\lambda)$  could be approximated by the relation  $S(\lambda) = 1424\lambda^{-0.409}$ ].

Equation 3 was checked by using the reflectance spectrum for a yellowish red hematite (SSA,  $17 \text{ m}^2 \text{ g}^{-1}$ ; Munsell color, 1.8YR 6.8/8.1) mixed in a 4 wt.% proportion with  $\text{BaSO}_4$ . As factor  $a$  increased, the hue became increasingly purple, the chroma decreased markedly, and value increased slightly. For  $a = 0.012$ , the calculated color was 7.2RP 8.4/2.6, which was similar to that for some coarse-grained synthetic hematites.

The relationship between value (*i.e.* lightness) and SSA is complex (Figure 9). Reflectivity seems to increase with decreasing SSA (increasing size) for samples with  $\text{SSA} < \sim 15 \text{ m}^2 \text{ g}^{-1}$ , as predicted by equation 3. This contradicts the common observation

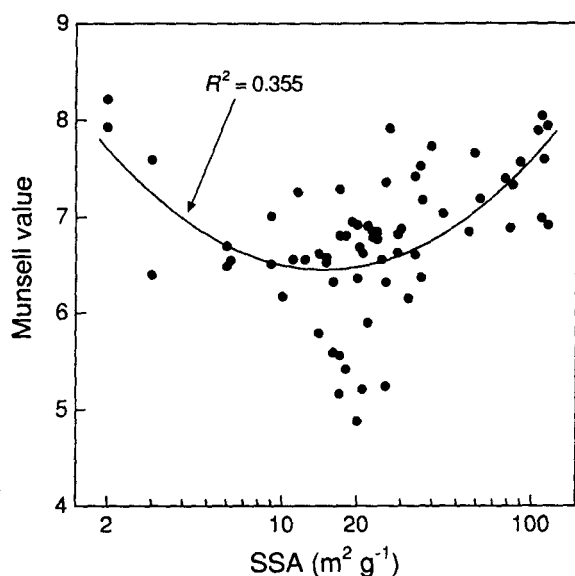


Figure 9. Munsell value in relation to specific surface area (SSA).

that purple, coarse-grained hematites are darker than fine-grained, red hematites when undiluted with a white standard. These contradictory observations can be reconciled by recalling that we used samples diluted with a white standard. In such a case, for the same mass proportion of hematite in the mixture, the total hematite surface capable of scattering light is inversely proportional to particle size. Therefore, with increasing dilution with a white standard, lightness increases more rapidly in coarse- than in fine-grained hematites.

Value increases with increasing SSA for  $\text{SSA} > \sim 15 \text{ m}^2 \text{ g}^{-1}$  (Figure 9), probably because (1) small hematite particles can cover most of the white standard and thus control scattering, and (2) the reflectivity of small particles increases with decreasing particle size in the wavelength region where absorption is low. This region, which corresponds to  $\lambda > \sim 550 \text{ nm}$ , is that which influences most markedly the  $Y$  value and hence lightness.

The weak correlations between SSA and color (and other spectral properties) are not unexpected because SSA depends not only on the size but also on the shape, surface roughness, and porosity of the particles. Therefore, one would expect  $\text{MCL}_{110}/\text{MCL}_{104}$ , which is a measure of the X-ray domain shape, to influence some spectral properties. However, the regression analysis does not support this idea, probably because this variable reflects the shape of the X-ray domains, but not necessarily that of the particles themselves.

Experimental evidence suggests that the actual scatterers in media made up of particles smaller than the wavelength are likely to be aggregated (Hapke, 1993). Thus, the red-bed samples studied by Torrent and Schwertmann (1987), also included in the present study, became yellower on grinding, which was interpreted as the result of the destruction of aggregates of small particles. Figures 8 and 9 indicated that the data points for red-bed samples are close to those for samples with similar SSA from other series. This suggests that hematite particles might also aggregate in the latter. However, the potential effect of aggregation on the hematite spectrum is difficult to evaluate experimentally.

#### Origin of the absorption bands

This study shows that some important crystal properties (SSA,  $\text{MCL}_{110}/\text{MCL}_{104}$  and, particularly, Al substitution) of hematite have a limited influence on the position of the  $\sim 545 \text{ nm}$  band. It must be added that the lack of strong correlations does not result from errors in establishing band position through the use of the second-derivative of the K-M function spectrum. For instance, if the intensity of the different bands are changed by manipulating the reflectance spectra according to equation 3, only slight changes in the position of the different bands in the second-derivative spectrum are observed.

Because the (weak) correlation between the position of the ~545 nm band and Al substitution contradicts the postulates of the ligand field theory, the assignment of this band to the  $2(6A_1) \rightarrow 2(4T_{1g}(4G))$  EPT raises serious doubts. The situation is similar to that of goethite: Scheinost *et al.* (1999) found shifts and splitting of the goethite band at ~485 nm assigned to analogous EPT by Sherman and Waite (1985) to contradict the postulates of the ligand field theory.

The presence of the ~485 nm band raises an even more difficult question. This band was not reported by Sherman and Waite (1985) and Scheinost *et al.* (1998), but was present in hematites with structural P (Gálvez *et al.*, 1999), and in Al hematites prepared by thermal treatment of lepidocrocite (van San *et al.*, 2001) or homogeneous precipitation of oxinates (da Costa *et al.*, 2002). According to Gálvez *et al.* (1999), the position of this band is the same as that of the band assigned to the goethite EPT by Sherman and Waite (1985), which is linked to  $Fe^{3+}-Fe^{3+}$  magnetic coupling between edge-sharing octahedra. This hypothetical 'goethite-like' EPT band in hematite was weaker than the EPT band at ~545 nm, which is linked to  $Fe^{3+}-Fe^{3+}$  magnetic coupling between face-sharing octahedra (a structural feature unique to hematite among Fe oxides). Gálvez *et al.* (1999) also observed that the ~485/~545 nm band intensity ratio increased with increasing Fe deficiency caused by incorporation of P and OH into the hematite structure, which would probably result in an increased ratio between edge-sharing and face-sharing octahedra. The same effect was observed in Al-substituted hematites by van San *et al.* (2001) and da Costa *et al.* (2002), as well as in some of the series studied in this work in which Al substitution was the main variable. However, our samples exhibited no correlation between the band intensity ratio and the degree of Al substitution, suggesting that factors other than Fe occupancy may govern the presence and intensity of this 'goethitic' EPT component. In conclusion, the hypothesis that the ~485 and ~545 nm bands correspond to the EPT for  $Fe^{3+}$  ions in contiguous edge- and face-sharing Fe octahedra, respectively, is attractive but inadequately supported by data currently available.

### CONCLUSIONS

The color of powdered hematite samples is related to the position and/or intensity of the main absorption bands in the visible spectrum, occurring at ~435, ~485 and ~535 nm. The properties of the last band seem to be influenced by the degree of Al substitution and the specific surface area of hematite, whereas none of the crystal properties considered in this study seems to influence the properties of the two other bands.

The results of this study cast serious doubts on the assignment of the ~535 nm band to the  $2(6A_1) \rightarrow 2(4T_{1g}(4G))$  electron pair transition (EPT), which relates

to the  $Fe^{3+}-Fe^{3+}$  magnetic coupling between face-sharing octahedra. They also show the common presence of the ~485 nm band, which can be tentatively assigned to a 'goethitic' structural component in Fe-defective hematite. Both topics merit consideration in any further study.

### ACKNOWLEDGMENTS

This research was supported by Spain's Ministry of Science and Technology (Project PB98-1015). We thank Prof. U. Schwertmann of the Technische Universität München for supplying some synthetic and natural hematite samples.

### REFERENCES

- Barrón, V. and Torrent, J. (1984) Influence of aluminum substitution on the color of synthetic hematites. *Clays and Clay Minerals*, **32**, 157–158.
- Barrón, V. and Torrent, J. (1986) Use of the Kubelka-Munk theory to study the influence of iron oxides on soil colour. *Journal of Soil Science*, **37**, 499–510.
- Barrón, V., Herruzo, M. and Torrent, J. (1988) Phosphate adsorption by aluminous hematites of different shapes. *Soil Science Society of America Journal*, **52**, 647–651.
- Burns, R.G. (1993) *Mineralogical Applications of Crystal Field Theory*, 2nd edition. Cambridge University Press, Cambridge, UK, 551 pp.
- Christensen, P.R., Bandfield, J.L., Clark, R.N., Edgett, K.S., Hamilton, V.E., Hoefen, T., Kieffer, H.H., Kuzmin, R.O., Lane, M.D., Malin, M.C., Morris, R.V., Peral, J.C., Pearson, R., Roush, T.L., Ruff, S.W. and Smith, M.D. (2000) Detection of crystalline hematite mineralization on Mars by the Thermal Emission Spectrometer: Evidence for near-surface water. *Journal of Geophysical Research*, **105**, 9623–9642.
- Colombo, C., Barrón, V. and Torrent, J. (1994) Phosphate adsorption and desorption in relation to morphology and crystal properties of synthetic hematites. *Geochimica et Cosmochimica Acta*, **58**, 1261–1269.
- Cornell, R.M. and Schwertmann, U. (1996) *The Iron Oxides*. VCH, Weinheim, Germany, 573 pp.
- Da Costa, G.M., Van San, E., De Grave, E., Vandenberghe, R.E., Barrón, V. and Datas, L. (2002) Al hematites prepared by homogeneous precipitation of oxinates: material characterization and determination of the Morin transition. *Physics and Chemistry of Minerals*, **29**, 122–131.
- Gálvez, N., Barrón, J. and Torrent, J. (1999) Preparation and properties of hematite with structural phosphorus. *Clays and Clay Minerals*, **47**, 375–385.
- Hapke, B. (1993) *Theory of Reflectance and Emittance Spectroscopy*. Cambridge University Press, New York, 455 pp.
- Kortüm, G. (1969) *Reflectance Spectroscopy*. Springer-Verlag, Berlin, 366 pp.
- Kubelka, P. and Munk, F. (1931) Ein Beitrag zur Optik der Farbanstriche. *Zeitschrift für technische Physik*, **12**, 593–620.
- Malengreau, N., Bedidi, A., Müller, J.-P. and Herbillon, A.J. (1996) Spectroscopic control of iron oxide dissolution in two ferrallitic soils. *European Journal of Soil Science*, **47**, 13–20.
- Morris, R.V., Lauer, H.V., Lawson, C.A., Gibson, E.K., Nace, G.A. and Stewart, C. (1985) Spectral and other physico-chemical properties of submicron powders of hematite ( $\alpha-Fe_2O_3$ ), maghemite ( $\gamma-Fe_2O_3$ ), magnetite ( $Fe_3O_4$ ), goethite ( $\alpha-FeOOH$ ), and lepidocrocite ( $\gamma-FeOOH$ ).

- Journal of Geophysical Research*, 90, 3126–3144.
- Morris, R.V., Schulze, D.G., Lauer, H.V., Agresti, D.G. and Shelfer, T.D. (1992) Reflectivity (visible and near IR), Mossbauer, static magnetic, and X-ray diffraction properties of Al-substituted hematites. *Journal of Geophysical Research*, 97, 10257-10266.
- Morris, R.V., Golden, D.C., Bell, III, J.F., Lauer, H.V.J. and Adams, J.B. (1993) Pigmenting agents in Martian soils: inferences from spectral, Mossbauer, and magnetic properties of nanophase and other iron oxides in Hawaiian palagonitic soil PN-9. *Geochimica et Cosmochimica Acta*, 57, 4597-4609.
- Morris, R.V., Golden, D. and Bell, III, J.F. (1997) Low-temperature reflectivity spectra of red hematite and the color of Mars. *Journal of Geophysical Research*, 102, 9125-9133.
- Press, W.H., Teukolsky, S.A., Vetterling, W.T. and Flannery, B.P. (1992) *Numerical Recipes in Fortran*, 2nd edition. Cambridge University Press, Cambridge, UK 963 pp.
- Scheinost, A.C. and Schwertmann, U. (1999) Color identification of iron oxides and hydroxysulfates: Use and limitations. *Soil Science Society of America Journal*, 63, 1463 — 1471.
- Scheinost, A.C., Chavernas, A., Barron, V. and Torrent, J. (1998) Use and limitations of second-derivative diffuse reflectance spectroscopy in the visible to near-infrared range to identify and quantify Fe oxides in soils. *Clays and Clay Minerals*, 46, 528-536.
- Scheinost, A.C., Schulze, D.G. and Schwertmann, U. (1999) Diffuse reflectance spectra of Al substituted goethite: a ligand field approach. *Clays and Clay Minerals*, 47, 156-164.
- Schwertmann, U., Friedl, J., Stanjek, H., Murad, E. and Bender Koch, C. (1998) Iron oxides and smectites from the Atlantis II Deep, Red Sea. *European Journal of Mineralogy*, 10, 953-967.
- Sherman, D.M. and Waite, T.D. (1985) Electronic spectra of Fe<sup>3+</sup> oxides and oxide hydroxides in the near IR to near UV. *American Mineralogist*, 70, 1262-1269.
- Torrent, J. and Schwertmann, U. (1987) Influence of hematite on the color of red beds. *Journal of Sedimentary Petrology*, 57, 682-686.
- Torrent, J., Schwertmann, U., Fechter, H. and Alferez, F. (1983) Quantitative relationships between color and hematite content. *Soil Science*, 136, 354-358.
- Van San, E., De Grave, E., Vandenberghe, R.E., Desseyn, H.O., Datas, L., Barron, V. and Rousset, A. (2001) Study of Al-substituted hematites, prepared from thermal treatment of lepidocrocite. *Physics and Chemistry of Minerals*, 28, 488-497.
- Wyszecki, G. and Stiles, W.S. (1982) *Color Science: Concepts and Methods, Quantitative Data and Formulae*. John Wiley & Sons, New York, 950 pp.

(Received 11 October 2002; revised 3 January 2003; Ms. 725)